Reversed Strength-ductility Relationship in Microstructurally Flexible High Entropy Alloy

S.S. Nene[a], M. Frank[a], K. Liu[a], S. Sinha[a], R.S. Mishra[a*], B. McWilliams[b], K.C. Cho[b]

[a]*Center for Friction Stir Processing, Department of Materials Science and Engineering, University of North Texas, Denton, Texas 76207 USA*

[b]*Weapons and Materials Research Directorate, U.S. Army Research Laboratory, Aberdeen Proving Grounds, MD 21005 USA*

**Corresponding author email: Rajiv.Mishra@unt.edu*

Conventional high strength alloys lack ductility due to lower work hardening and early onset of damage nucleation. To overcome this deficiency, high entropy alloys (HEAs) enjoy the benefit of metastabillity of phases to tune the deformation mechanisms for engineering strength and ductility. Inspired by this, here we present friction stir processed $Fe_{40}Mn_{20}Co_{20}Cr_{15}Si_5$ HEA with ultrafine face centered cubic (f.c.c.) γ grains embedded in a refined hexagonal closed packed (h.c.p) ε matrix. Transformation of γ grains and twinning in ε matrix triggered uniform strain partitioning among these phases and sustained work hardening during deformation thereby reversing the conventional strength-ductility trade-off.

Keywords: Strength; Ductility; Strain-Induced Transformation; Twinning; High Entropy Alloy

Strength and ductility are basic fundamental properties that determine the usability of a structural material. However, strength always varies inversely with ductility; thus, the popularly known phrase "inverse strength-ductility relationship" in metallic materials is considered as the crucial factor in alloy design [1-2]. Major research efforts [1-5] are targeted on overcoming this inverse strength-ductility trade-off through development of advanced materials such as ultra-high strength steels, aluminium alloys and recently-explored high entropy alloys (HEAs). The concept of adding equal amounts of constituent elements in the alloy system led to the foundation of well-known CoCrMnFeNi equiatomic HEAs that showed exceptional room temperature mechanical properties [2, 3]. Further work on HEA compositional design by addition of non-transition element such as Al in the equiatomic configuration resulted in significant improvement not only in tensile behaviour but

also in wear, corrosion and fatigue properties of the alloy [4-8]. The latest work by Li *et al.* [9] utilized the metastabillity of phases synergized with high entropy to tune the deformation mechanisms and thereby yield an extraordinary combination of strength and ductility for non-equiatomic dual-phase HEAs (DP-TRIP-HEAs). Thus, they claimed that the material can be ductilized with steady increase in strength through sustained work hardening (WH) during deformation. Classical theory of WH considers dislocation-based hardening as the major component in enhancing strength. However, microstructural features such as precipitates, deformation twins, and strain-induced phases become predominant in strain accommodation depending on the stacking fault energy (SFE) of the material [9-11]. Non equiatomic design of HEAs provides huge compositional space for developing new alloys with tunable SFEs that upon subsequent processing show responsive microstructural evolution. This responsive microstructural evolution in conjunction with core benefits of HEAs provide adaptive phase stability in the alloy for obtaining the desired property combination. This "Microstructural Flexibility" in an alloy can be very useful for overcoming the conventional strength-ductility dilemma [1, 9-11]. He *et al.* [1] postulated that severe plastic deformation (SPD) of austenitic matrix in transformation induced plasticity (TRIP) steels gives rise to first-order, strain-induced austenitic (f.c.c) to martensitic (h.c.p.) transformation that results in highly dislocated martensitic matrix in the microstructure. However, along with dislocated martensite (ε, h.c.p. phase), the SFE-governed phase stability triggers different strain accommodation modes in the material providing simultaneous increase in strength and ductility [1, 9]. To favour twinning induced plasticity (TWIP) or TRIP in the material, SFE should be low enough to decrease either the critical stress required for twinning or martensitic start (M_S) temperature [10-14]. As Si and Cr were reported to decrease the SFE [12-14] in the Fe-Mn rich alloys, a new HEA $Fe_{40}Mn_{20}Co_{20}Cr_{15}Si_5$ (all in at.%) was developed to incorporate the possibility of transformation or twin driven plasticity in the material via reduction in SFE (i.e. increasing the metastabillity of γ (f.c.c.) phase). Therefore, this enhanced metastabillity of γ phase in these TRIP/TWIP alloys provides temperature, strain and/or strain rate sensitive phase evolution in the material during processing [12-14]. Conventional processing such as rolling, forging can control either of the temperature or strain rate during one cycle whereas simultaneous control of temperature, strain rate and strain during processing would provide the responsive phase and grain size evolution (i.e. microstructural flexibility) in the material having particular chemistry. Friction stir processing (FSP) being a unique process wherein all these processing parameters can be controlled in synergy [15], was thus used to engineer the microstructure

of the $Fe_{40}Mn_{20}Co_{20}Cr_{15}Si_5$ (henceforth designated as CS-HEA) HEA in the present work.

The CS-HEA was produced by vacuum arc-casting in a cold-copper crucible. The vacuum level achieved was approximately 300 μm, and the chamber was backfilled with argon to 1 atm prior to each melt using pure metals with a nominal composition of $Fe_{40}Mn_{20}Co_{20}Cr_{15}Si_5$ (at %) and ingot dimensions of $300 \times 100 \times 6$ mm^3. Subsequently, these 6 mm sheets were friction stir processed (FSP) using the W-RE tool with the parameters as shown in Table 1. The processing tool had a shoulder diameter of 12 mm with tapered pin. The root diameter, pin diameter, and length of the tool were 7.5 mm, 6 mm, and 3.5 mm, respectively.

Microstructure of the alloy in as-cast (coarse-grained) and recrystallized (grain-refined) conditions were analyzed by various methods. X-ray diffraction (XRD) measurements were performed using an RIGAKU X-Ray equipped with Cu K_α radiation operated at 40 kV and 30 mA. Electron backscatter diffraction (EBSD) measurements were carried out by a FEI NOVA Nano (SEM) with a Hikari camera and the data was analyzed using TSL OIM 8 software. Dislocation density measurements were made using the TSL software which follows the procedure mentioned in Ref. [16]. Rectangular 1 mm-thick, dog-bone-shaped mini-tensile specimens were machined using a mini computer numerical control (CNC) machine from 1 mm below the surface within the nugget region of the all FSP specimens, whereas from the top surface of the as-cast ingot. Gage length and width of the tensile specimens were 5 and 1.25 mm, respectively. In each condition, three samples were tested at room temperature and an initial strain rate of 10^{-3} s^{-1} to confirm reproducibility of the results.

As expected, the selection of alloy chemistry lowered the SFE substantially thereby stabilizing the ε phase dominant dual phase microstructure [12-14] in the as-cast condition of CS-HEA (Fig. 1a-1e). The chemical homogeneity of the microstructure is also evident from the EDS-X-ray map for as-cast material (Fig. 1b) depicting elemental composition very similar to nominal composition (NC) of CS-HEA (Fig. 1c). The grain size as well as martensite (ε) phase fraction prior to deformation in the as-cast material is the characteristic of the chemistry of the alloy [9-11] which further gets altered by the processing (Fig. $1f_1$ - $1f_3$).

The intense deformation per unit time (i.e. strain rate) at higher temperature refines ε phase while short duration does not allow complete transformation to γ phase which is thermodynamically

stable phase at high temperature. This kinetic stabilization (strain, strain rate and temperature sensitive phase stability) of phases while refining the microstructure is key for producing flexible microstructures in the material [10, 13]. Similar observations are made in the present study (Fig. $1f_1$ - $1f_3$) wherein S350 (single pass of FSP at 350 rotations per minute (RPM)) specimens (i.e. high strain rate processing) showed almost 90% ε phase (Fig. 1d - 1e and $1f_1$); whereas S150 (single pass of FSP at 150 RPM) condition (i.e. low strain rate processing) exhibited γ phase (65%) dominant dual phase microstructure (Fig. 1d - 1e and $1f_3$). The microstructural evolution in D-pass (two overlapping passes, first at 350 followed by 150 RPM run) specimen is quite different from S150 even though the final thermomechanical processing experienced by both specimens is similar. This is a strong indication of the deformation induced phase stability during the 350 RPM run which altered the microstructural evolution in CS-HEA during the subsequent 150 RPM run. Moreover, almost equal <c+a> dislocation density value of ~ 5×10^{14} m^{-2} for both S350 and S150 conditions indicates that D-pass has experienced almost similar strain at the end of processing but with higher heat input which drives the formation of almost 31% γ phase (Fig. $1f_2$) at the end of the second pass in D-pass condition [9,11,17]. These results suggest that, CS-HEA showed responsive phase evolution with FSP parameters suggesting plausibility of microstructural flexibility in the same. Though, there is responsive microstructural evolution upon FSP, the chemical homogeneity of the material is unaltered due to shear driven transport of elements during processing [15]. The EDS analysis for the D-pass specimen (Fig. 1c) confirms the chemically homogenized microstructure by showing the elemental distribution very close to the nominal composition of CS-HEA.

Conventional materials including TRIP steels [18, 19] show increased strength with deterioration of ductility as depicted by the blue and yellow curves in Fig. 2a. However, CS-HEA exhibited a completely reversed trend exhibiting higher ductility for specimens with higher strength (marked by the red curve in Fig. 2a. This reversal in the strength-ductility relationship is attributed to the self-tunable deformation accommodation in microstructurally flexible CS-HEA. This is also confirmed by the distinct nature of engineering stress-engineering strain curves (Fig. 2b) for each FSP condition in comparison with the as-cast state. The as-cast material contained coarse grained ε phase (Fig. 1a), which limits its WH ability since forming geometrically necessary dislocation (GND) arrays in harder and larger martensitic matrix is not favorable and hence exhibit low strength and ductility [2]. Up to ~100% increase in yield strength (YS) upon FSP can be attributed to reduction of ε and γ grain sizes

(average d ~0.5-0.6 μm). In TRIP steels, strain induced martensitic transformation is the primary mode for plasticity [9, 18, 19] whereas in most of the conventional materials, slip dominant dislocation interactions accommodates most of the strain [9-11]. However, the extent of WH in FSP-CS-HEA specimens during tensile deformation is primarily driven by the prior ε and γ phase fractions and their distribution in the microstructure.

Detailed characteristics of deformation related changes in microstructure are shown in Fig. 3a - 3f). Figs. 3b - 3e have three corresponding micrographs capturing phase distribution, orientation distribution and GND distribution for S350 and D-pass specimens before and after deformation. The starting microstructure of S350 condition showed twinned martensitic microstructure along with very fine γ phase dispersed throughout it (Fig. $3b_1$). Being h.c.p. lattice, martensite (ε phase) has fewer slip systems available for deformation than the γ phase and thus undergoes pronounced twinning and pyramidal <c+a> slip to accommodate deformation (compare the GND distribution in Figs. $3b_3$ and $3c_3$). S350 condition depicted a rapid decrease during stage III of WH with localized variation in slope of the curve over a narrow plastic strain range of 0.05 to 0.15 (green curve in Fig. 3a). Indication of controlled deformation twinning in ε phase for S350 is further highlighted by black arrows in Figs. $3c_1$ and $3c_2$. Overall uniformity of GND distribution (Fig. $3c_3$) across twinned and un-twinned regions is evident. The S350 condition had very high starting ε phase fraction, so no substantial change in the ε phase fraction during tensile deformation (Figs. $3b_1$ and $3c_1$)) is expected. Therefore, TWIP in ε phase is a primary mode of deformation for S350 condition [9, 11, 20 - 22].

D-pass condition showed distinctly different WH behavior by the gradual change in slope at the strain level of ~0.08 with the formation of the local maxima (hump) at later stages of tensile deformation (Fig. 3a). This notable slope change in the WH curve is a strong indication of TRIP which is supported by the evolution of as-processed dual phase microstructure (Fig. $3d_1$) to fully martensitic microstructure (Fig. $3e_1$). The formation of hump in the red curve (Fig. 3a) represents a local increase in WH rate because of dynamic Hall-Petch effect associated with formation of twins in the pre-existing and transformed ε phase [9-11]. As marked with black arrows in Figs. $3e_1$ and $3e_2$, extensive deformation twinning occurred in ε phase field supporting the local increase in the WH rate over strain of 0.08 to 0.17 due to twinning. Moreover, the uniform GND density spread in twinned and transformed regions of the microstructure (Fig. $3e_3$) is a validation towards synergistic contribution of both TRIP and TWIP mechanisms in strain accommodation for D-pass condition. Fig.

3f provides the <c+a> dislocation density distribution for both S350 and D-pass conditions in as-processed and deformed states. It is clear that both the conditions had similar GND density stored upon FSP which supports the fact that the phase evolution in both of them is driven by the temperature and strain rate [1, 11, 20-21]. Moreover, the D-pass specimen provided more controlled work hardening as compared to S350 condition upon tensile deformation due to higher GND density (Fig. 3f) in former by 0.36×10^{15} m^{-2}. These results make it clear that invoking microstructural flexibility in the material is not only dependent on chemistry of the alloy but also on the processing route adopted to facilitate it.

Figures 4a and 4b compare the YS and uniform elongation as a function of ε phase fraction obtained in the microstructure prior to tensile deformation for CS-HEA and all other DP-TRIP-HEAs reported till date. It is apparent from Fig. 4a that CS-HEA outperforms all DP-TRIP-HEAs in the YS values thereby showing almost highest YS of ~780 MPa for S350 condition. Also, CS-HEA showed highest prior ε fraction irrespective of processing condition which is attributed to the adaptive phase stability with strain, strain rate and temperature (i.e. microstructural flexibility) which is not seen in widely developed advanced TRIP steels [1, 22] or DP-TRIP-HEAs. Another distinct outcome is the substantial uniform elongation of 25% for S350 condition in spite of having almost 90% prior ε phase fraction. This is attributed to the ability of this ε phase to undergo <c+a> slip as well as twinning simultaneously during deformation thereby making it more damage tolerant. In short, microstructural flexibility in CS-HEA leads to the simultaneous increase in YS and UTS while attaining comparable uniform elongation (D-pass condition) on comparison to DP-TRIP-HEAs reported in the literature [9, 11, 23].

In summary, friction stir processed CS-HEA shows microstructural pathways for obtaining exceptional combination of strength and ductility. The refined martensitic matrix in conjunction with γ (f.c.c.) phase provides flexibility to the microstructure in undergoing controlled transformation and twinning-induced plasticity. Interestingly, CS-HEA with almost 90% prior ε phase fraction also showed reasonable uniform elongation (25 %) with exceptionally high YS (~ 784 MPa) and UTS (~ 1.13 GPa) in comparison with its DP-TRIP-HEA counterparts. Thus, by designing a flexible microstructure, we conquered the traditional strength-ductility trade-off paradigm.

References

[1] B. B. He, B. Hu, H.W. Yen, G.J. Cheng, Z.K. Wang, H.W. Luo, M. X. Huang, Science 357 (2017) 1029.

[2] J. Yeh, S.K. Chen, S. Lin, J. Y. Gan, T.S. Chin, T.T. Shun, C.H. Tsau, S.Y. Chang, Adv. Eng. Mater. *6* (2004) 299.

[3] D.B. Miracle, O.N. Senkov, Acta Mater. 122 (2017) 448.

[4] J.W. Yeh, S.-K. Chen, J.-Y. Gan, S.-J. Lin, T.-S. Chin, T.-T. Shun, C.-H. Tsau, S.-Y. Chou, Metall. Mater. Trans. A 35(8) (2004) 2533.

[5] L.J. Santodonato, Y. Zhang, M. Feygenson, C.M. Parish, M.C. Gao, R.J.K. Weber, J.C. Neuefeind, Z. Tang, P.K. Liaw, Nature Comm. 6 (2015) 5964.

[6] M.H. Chuang, M.H. Tsai, W.R. Wang, S.J. Lin, J.W. Yeh, Acta Mater. 59 (2011) 6308.

[7] M.A. Hemphill, T. Yuan, G.Y. Wang, J.W. Yeh, C.W. Tsai, A. Chuang, P.K. Liaw, Acta Mater. 60 (2012) 5723.

[8] Y. Shi, B. Yang, X. Xie, J. Brechtl, K.A. Dahmen, P.K. Liaw, Corr. Sci. 119 (2017) 33.

[9] Z. Li, C.C. Tasan, K.G. Pradeep, D. Raabe, Acta Mater. 131 (2017) 323.

[10] B. C. De Cooman, Y. Estrin, S. K. Kim, Acta Mater. 142 (2018) 283.

[11] S. S. Nene, K. Liu, M. Frank, R.S. Mishra, R.E. Brennan, K. Cho, Z. Li, D. Raabe, Sci. Reports *7* (2017) 16167.

[12] R. Xiong, H. Peng, H. Si, W. Zhang, Y. Wen, Mater. Sci. Eng. A. 598 (2014) 376.

[13] E. I. Galindo-Nava, P. E. J. Castillo, Acta Mater. 128 (2017) 120.

[14] C. Ghosh, C. Aranas, JJ. Jonas, Prog. Mater. Sci. 82 (2016) 151.

[15] S. Palanivel, A. Arora, K.J. Doherty, R.S. Mishra, Mater. Sci. Eng. A 678 (2016) 308.

[16] D. Field, C. C. Merriman, I. N. Mastorakos, Sol. St. Phen. 160 (2010) 17.

[17] P. Escobar, D. Silva, D. S. Ferreira, D. Santos, J. Mater. Res. Technol. 4 (2015) 162.

[18] Z. J. Long, X. Yan, S. Wen, L. Lin, J Iron Steel Res. Intl. 19 (2012) 57.

[19] K. Zhua, C. Magera, M. Huang, J. Mater. Sci. Tech. 33 (2017) 1475.

[20] M. Calcagnotto, D. Ponge, E. Demir, D. Raabe, Mater. Sci. Eng. A 527 (2010) 2738.

[21] S. H. Kim, H. Kim, N. J. Kim, Nature 518 (2015) 77.

[22] S. Jiang, H. Wang, Y. Wu, X. Liu, H. Chen, M. Yao, B. Gault, D. Ponge, D. Raabe, A. Hirata, Nature 544 (2017) 460.

[23] M. Frank, S.S. Nene, K. Liu, R.S. Mishra, R.E. Brennan, K. Cho, Z. Li, D. Raabe, Manuscript submitted for publication (2018).

Acknowledgments

The work was performed under a cooperative agreement between the Army Research Laboratory and the University of North Texas (W911NF-13-2-0018). The authors are thankful to the Center for Advanced Research and Technology for providing access to the microscopy facilities at the University of North Texas. Authors would also like to acknowledge the help by J. Jacobson, S. Zellner and J. Reeder in EBSD and tensile sample preparation.

Declaration of interests: None.

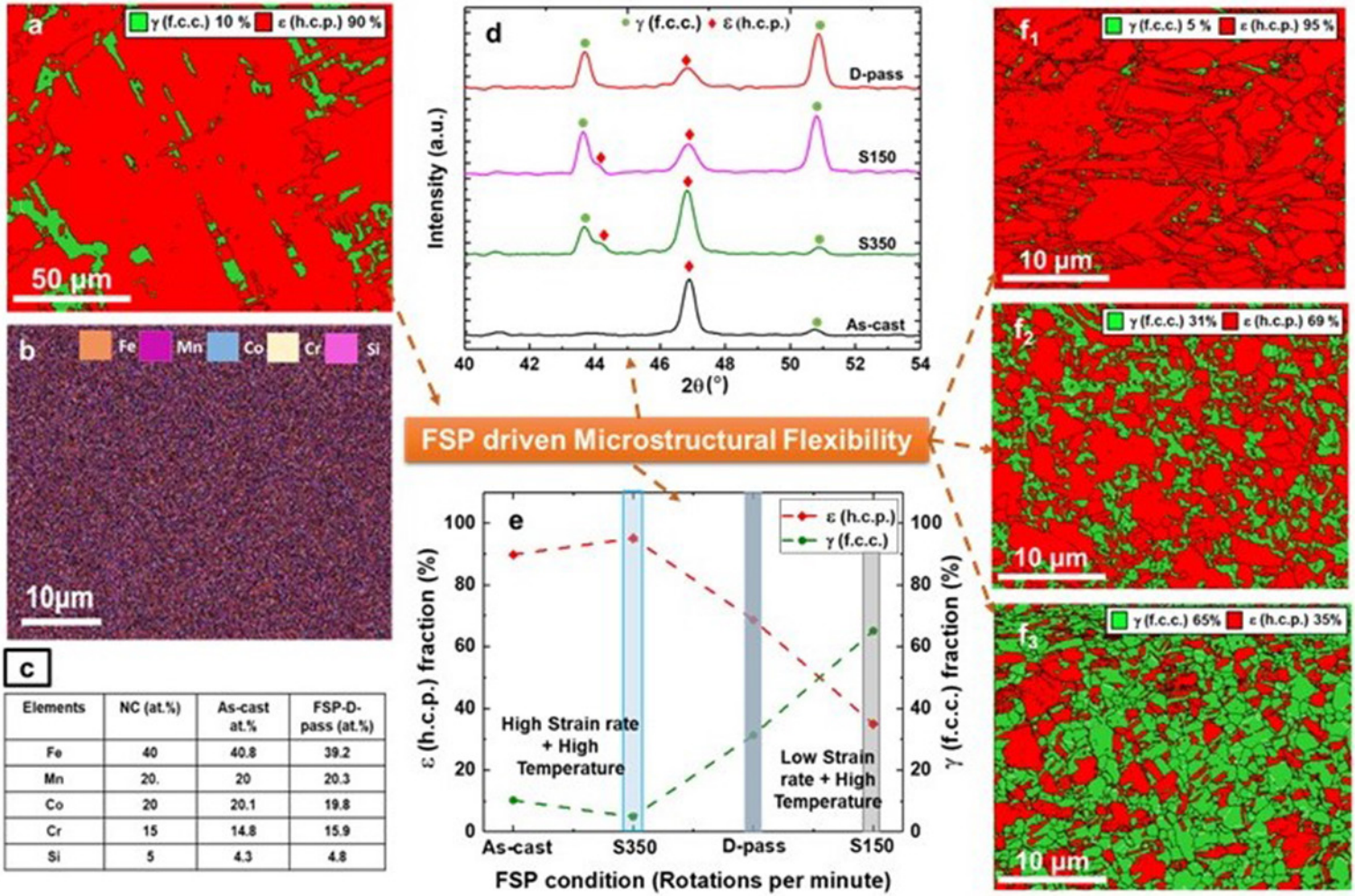

c

Elements	NC (at.%)	As-cast at.%	FSP-D-pass (at.%)
Fe	40	40.8	39.2
Mn	20.	20	20.3
Co	20	20.1	19.8
Cr	15	14.8	15.9
Si	5	4.3	4.8

Fig. 1. Microstructural evolution in CS-HEA upon FSP. (a-b) As-cast microstructure with corresponding EDS-X-ray map showing chemical homogeneity. (c) EDS elemental distribution for as-cast and D-pass specimens. (d) X-ray diffraction analysis for all processing conditions. (e) ε (h.c.p.) and γ (f.c.c.) phase fractions plotted with all FSP parameters; EBSD phase maps for (f_1) S350, (f_2) D-pass, and (f_3) S150 conditions respectively. (NC: nominal composition of CS-HEA; FSP: friction stir processing; EBSD: electron back scattered diffraction).

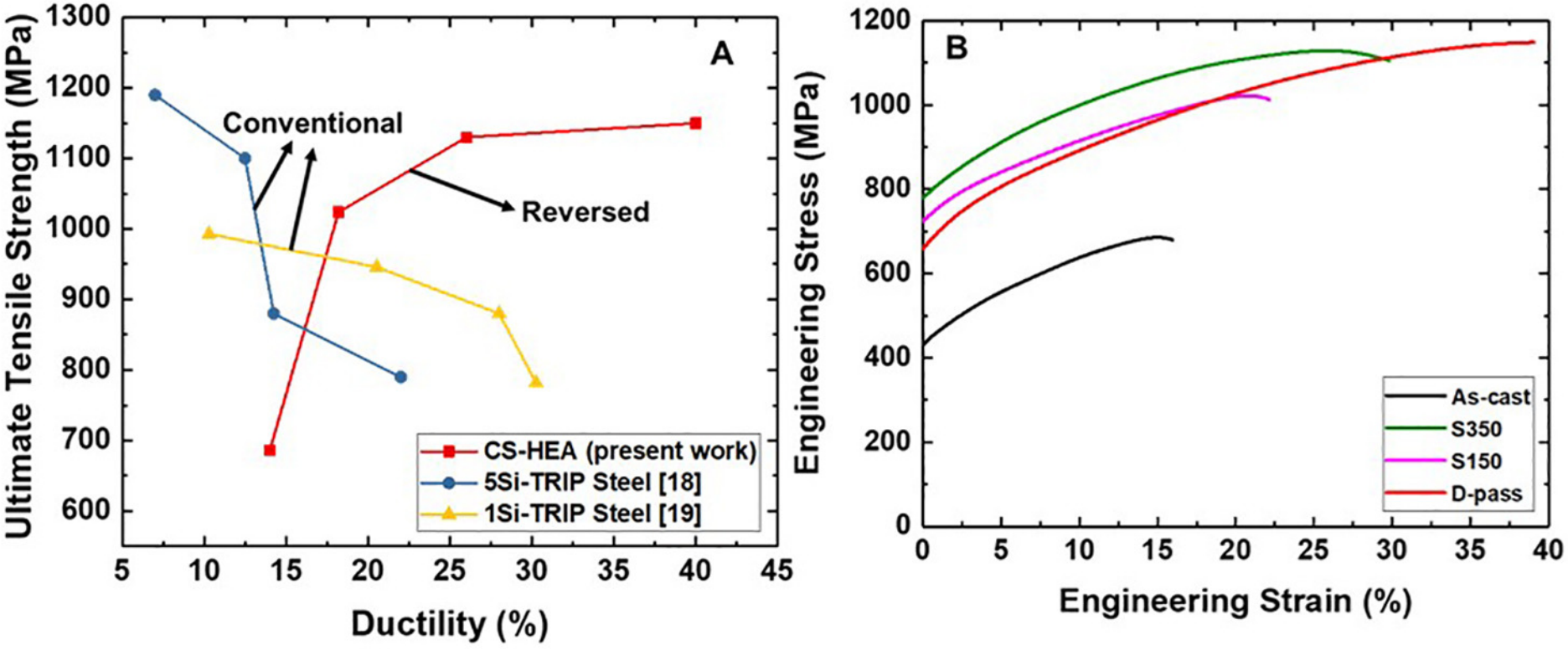

Fig. 2. Tensile properties of CS-HEA upon FSP. (a) Reversed strength-ductility behavior in CS-HEA compared to its counterparts; i.e., TRIP steels [18, 19]. (b) Engineering stress-strain curves for all FSP conditions in comparison with as-cast material.

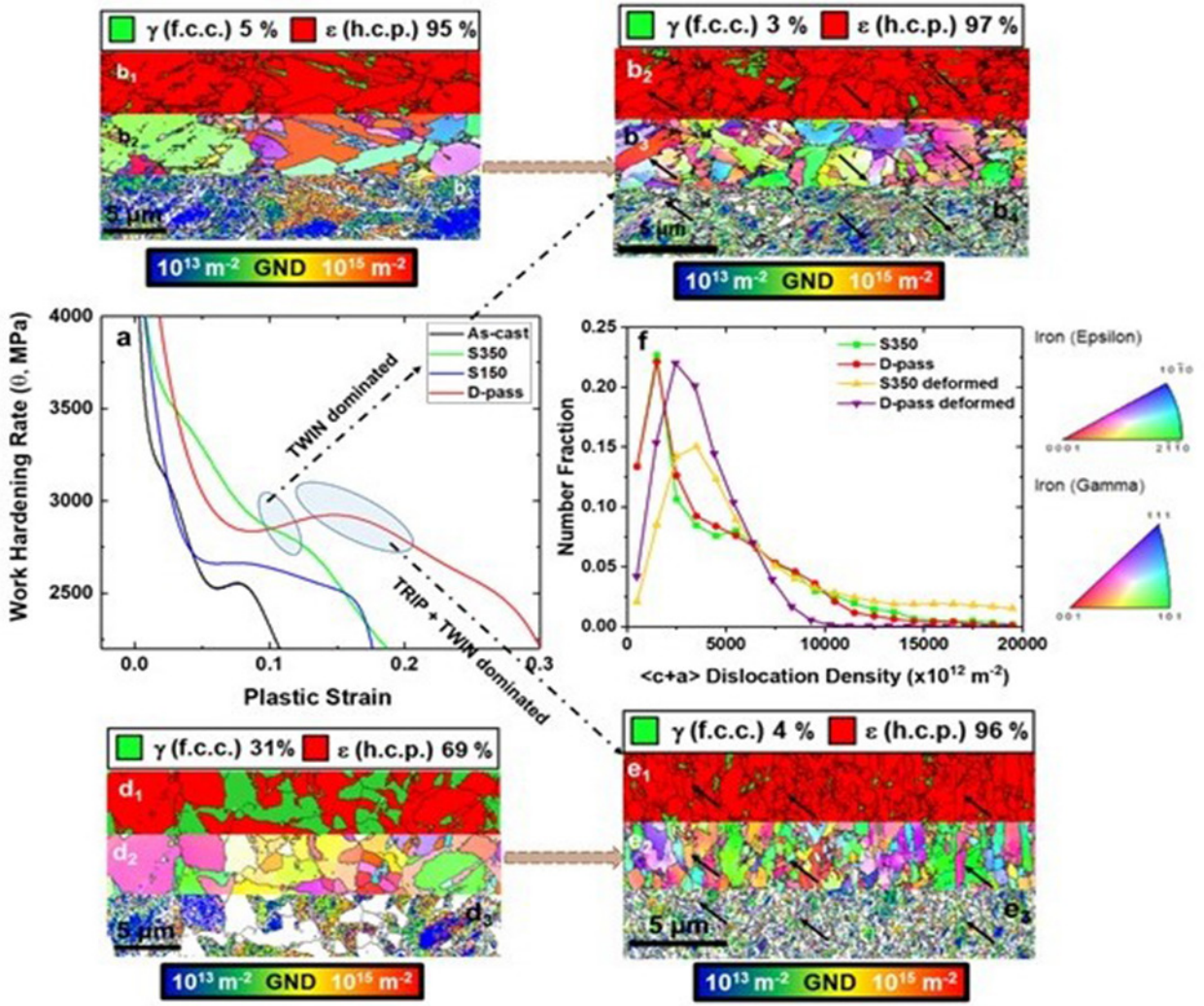

Fig. 3. Deformation mechanisms in CS-HEA. (a) Work hardening rate (θ) vs plastic strain for all processing conditions. EBSD maps depicting (X_1: Phase; X_2: IPF; X_3: GND): ($b_1 - b_3$) for as processed S350 condition. ($c_1 - c_3$) for S350 condition after tensile deformation. ($d_1 - d_3$) for as-processed D-pass condition. ($e_1 - e_3$) for D-pass condition after tensile deformation. (f) <c+a> dislocation density distribution for S350 and D-pass conditions. (EBSD: electron back scattered diffraction; IPF: inverse pole figure; GND: geometrically necessary dislocation).

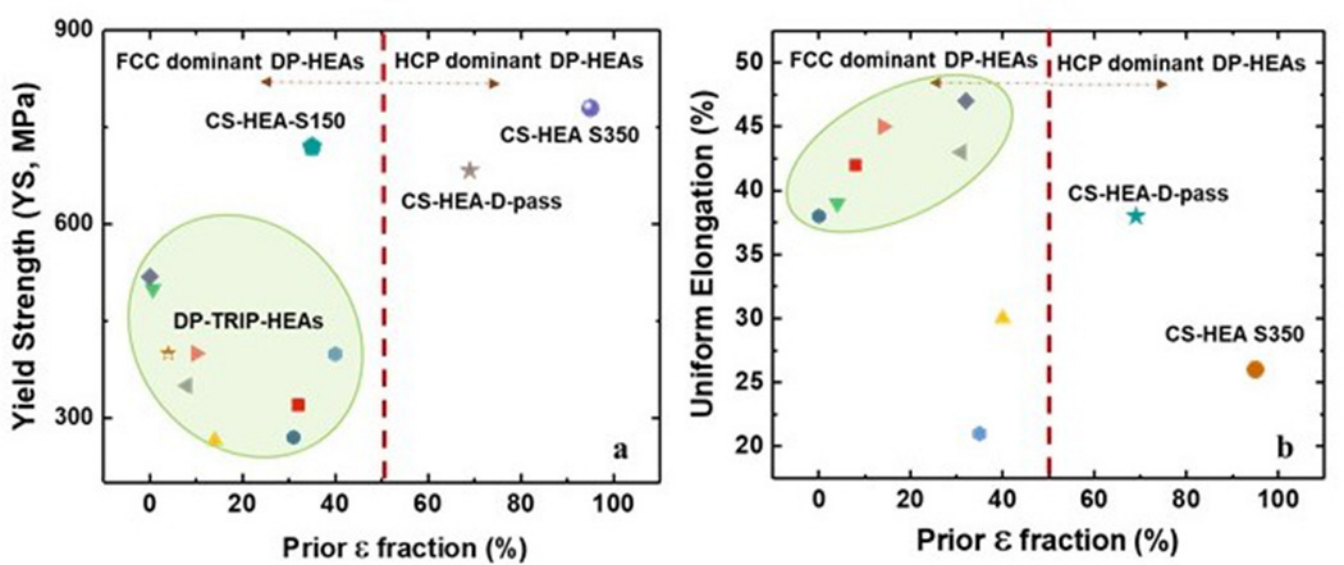

Fig. 4. (a) YS and (b) uniform elongation plotted as a function of ε phase fraction in the microstructure prior to tensile deformation for grain refined CS-HEA and all DP-TRIP-HEAs (grain refined) reported till date [2, 6, 19].

Table 1: Processing parameters selected for FSP.

Processing parameters	**S350**	**S150**	**D-pass**	
	Single pass	**Single pass**	**Pass 1**	**Pass 2**
Rotational Rate (RPM)	350	150	350	150
Traverse Speed (mm/min)	50.8	50.8	50.8	50.8
Plunge Depth (mm)	3.65	3.65	3.65	3.65
Tilt Angle (°)	2.0	2.0	2.0	2.0

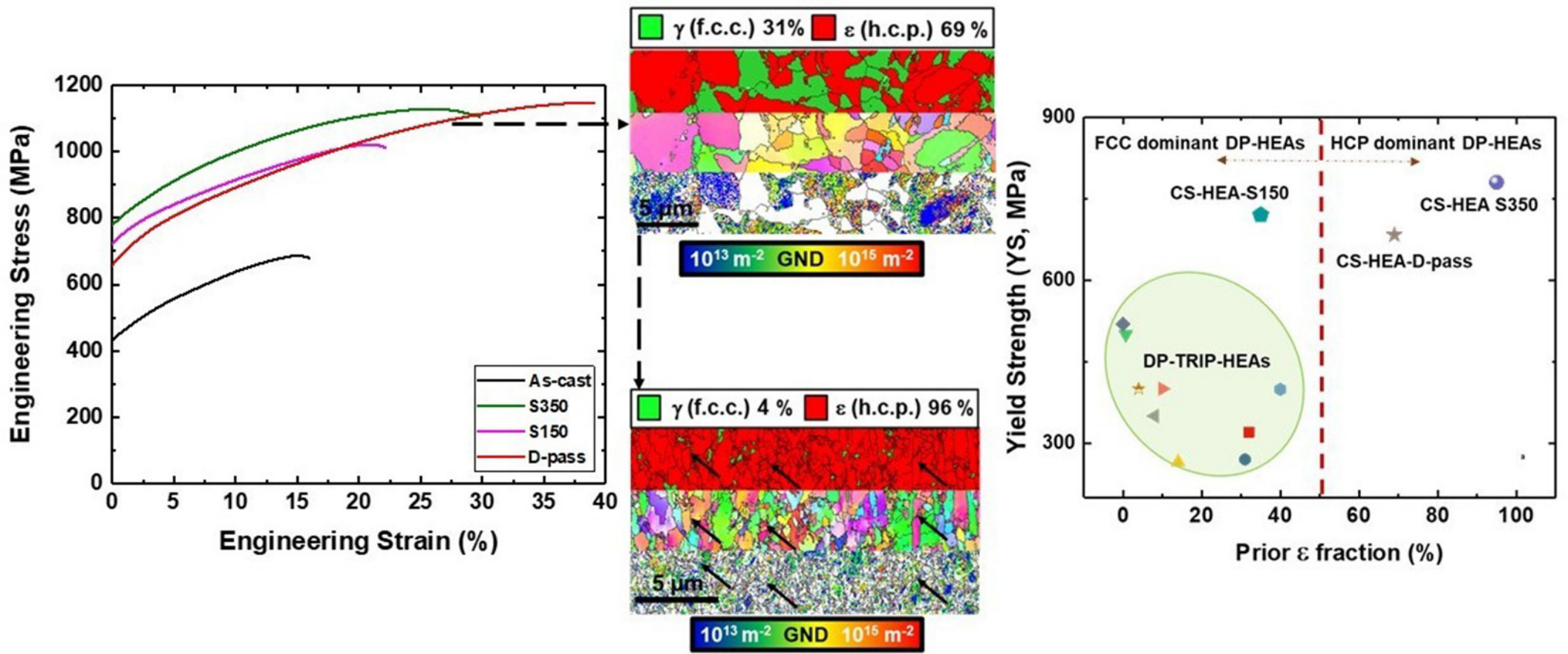
Engineering Stress (MPa)
Engineering Strain (%)
As-cast
S350
S150
D-pass
γ (f.c.c.) 31%
ε (h.c.p.) 69 %
5 μm
10^13 m^-2 GND 10^15 m^-2
γ (f.c.c.) 4 %
ε (h.c.p.) 96 %
5 μm
10^13 m^-2 GND 10^15 m^-2
Yield Strength (YS, MPa)
Prior ε fraction (%)
FCC dominant DP-HEAs
HCP dominant DP-HEAs
CS-HEA-S150
CS-HEA S350
CS-HEA-D-pass
DP-TRIP-HEAs